Journal of Physics: Conference Series **702** (2016) 012012 doi:10.1088/1742-6596/702/1/012012

Conventional and Unconventional Pairing and Condensates in Dilute Nuclear Matter

John W Clark[1,2], Armen Sedrakian[3], Martin Stein[3], Xu-Guang Huang[4], Victor A Khodel[1,5], Vasily R Shaginyan[6], Mikhail V Zverev[5,7]

[1] Department of Physics and McDonnell Center for the Space Sciences, Washington University, St. Louis, MO 63130 USA
[2] Center for Mathematical Sciences, University of Madeira, Funchal, 9000-390 Portugal
[3] Institute for Theoretical Physics, J. W. Goethe-University, D-60438 Frankfurt am Main, Germany
[4] Physics Department & Center for Particle Physics and Field Theory, Fudan University, Shanghai 200433, China
[5]National Research Centre Kurchatov Institute, Moscow, 123182, Russia
[6] Petersburg Nuclear Physics Institute, NRC Kurchatov Institute, Gatchina, 188300, Russia
[7] Moscow Institute of Physics and Technology, Dolgoprudny, Moscow District 141700, Russia

E-mail: jwc@wuphys.wustl.edu

Abstract. This contribution will survey recent progress toward an understanding of diverse pairing phenomena in dilute nuclear matter at small and moderate isospin asymmetry, with results of potential relevance to supernova envelopes and proto-neutron stars. Application of *ab initio* many-body techniques has revealed a rich array of temperature-density phase diagrams, indexed by isospin asymmetry, which feature both conventional and unconventional superfluid phases. At low density there exist a homogeneous translationally invariant BCS phase, a homogeneous LOFF phase violating translational invariance, and an inhomogeneous translationally invariant phase-separated BCS phase. The transition from the BCS to the BEC phases is characterized in terms of the evolution, from weak to strong coupling, of the pairing gap, condensate wave function, and quasiparticle occupation numbers and spectra. Additionally, a schematic formal analysis of pairing in neutron matter at low to moderate densities is presented that establishes conditions for the emergence of both conventional and unconventional pairing solutions and encompasses the possibility of dineutron formation.

1. Introduction

This report serves to review and analyze a body of recent findings on the phase diagram of dilute nuclear matter, calculated over wide ranges of density, temperature, and isospin asymmetry. Quantitative results will be presented for the temperature-density ($T - \rho$) phase diagram at baryon densities below about half the saturation density of isospin-symmetric nuclear matter, but pairing phenomena that may occur at somewhat higher densities will also be addressed. The corresponding studies [1, 2, 3, 4, 5], both theoretical and numerical, focus attention on the emergence of unconventional as well as conventional pairing in the ${}^3S_1$-${}^3D_1$ (deuteron) channel as well as associated BCS-BEC crossovers. Earlier work on these and closely related themes has been described in [6, 7, 8, 9, 10, 11] and more recently in [12, 13, 14, 15, 17, 18, 19].

Application of *ab initio* quantum many-body theory to this problem domain has the distinct advantage that, within the density regime considered in the numerical study, the two-body nucleon-nucleon (NN) interactions are well constrained by the NN phase-shift data and the properties of the deuteron. Nor is the problem purely academic, as it is directly relevant to the matter existing in supernovae envelopes and proto-neutron stars (having relatively low temperatures and low isospin asymmetries) and in neutron star crusts (cold, with large isospin asymmetries).

The complex phenomenology of dilute nuclear matter, summarized in its $T-\rho$ phase diagram determined over a range of isospin asymmetries, arises from three sources:

(1) Pauli exclusion acting for fermionic species (nucleons, tritons, ^{3}He, etc.) and Bose-Einstein condensation (BEC) of bosonic species (such as deuterons and alpha particles). These are most effective at high particle densities (but below nuclear saturation), low temperatures, and low mass number of nuclear species.

(2) Dominance of the longer-range attractive component of the NN interaction. At low densities and not-so-low temperatures, this component is responsible for the formation of tightly bound nuclear clusters (deuterons, dineutrons(?), tritons, alphas, ...), which can undergo BEC in the case of bosonic clusters. At higher densities and low temperatures it is responsible for the formation of Cooper pairs with pairing gap Δ. At small isospin asymmetries the pairing is in the triplet $^3S_1$-$^3D_1$ channel, whereas for large asymmetries the pairing is in the $^1S_0$ singlet channel.

(3) Isospin asymmetry, induced by weak interactions, producing a mismatch of neutron (n) and proton (p) Fermi momenta, giving rise to mixed superfluid/normal phases and unconventional pairing − Cooper pairs with nonzero center-of-mass (CM) momentum (the so-called LOFF phase [20]) or deformed neutron and proton Fermi surfaces [21].

2. Phase Diagram of Dilute Isospin-Symmetric Nuclear Matter

We begin with a brief examination of the low-density phase diagram for the fiducial case of isospin-symmetric nuclear matter with equal neutron and proton baryon densities, $\rho_n = \rho_p$, as explored in [1]. A model of low-density nuclear matter based on a simplified two-nucleon interaction was considered which exhibits behavior generic to systems of fermions interacting via a short-range repulsion and a longer-range attraction. Such behavior includes both (i) formation of clusters tightly bound in the medium at lower densities and higher temperatures, and (ii) Cooper pairing in a BCS state at lower temperatures and higher densities. Specifically, a Malfliet-Tjon model with MF-III parametrization [22] was chosen for the NN interaction, consisting of a central but spin-dependent superposition of inner repulsive and outer attractive Yukawas, fitted to NN S-wave phase shifts and deuteron binding. This interaction shows a strong pairing instability in the $^3S_1$ channel.

To study the low-temperature superfluid phase, the BCS gap equation was solved self-consistently for the energy gap $\Delta(T)$ and the chemical potential μ below the critical temperature T_{sc}, with results shown in Fig. 1. Proceeding from higher to lower densities in the domain under study, conditions range from weak coupling (WC) to strong coupling (SC) as measured by the ratio $\Delta(0)/|\mu|$; a change of sign of the chemical potential from positive to negative is a signature of the WC $\rightarrow$ SC transition. In the low-ρ limit the gap equation reduces to the Schrödinger equation for the two-body bound state, with energy eigenvalue given by 2μ, which is naturally identified with the deuteron and subject to Bose-Einstein condensation. Accordingly, this earlier study provides a model of the BCS-BEC transition from BCS Cooper pairing in the $^3S_1$ state to a Bose condensate of simplified deuterons.

To extend the phase diagram to higher temperatures, the Lippmann-Schwinger and Faddeev equations were adapted to solve two- and three-nucleon bound-state problems in the presence

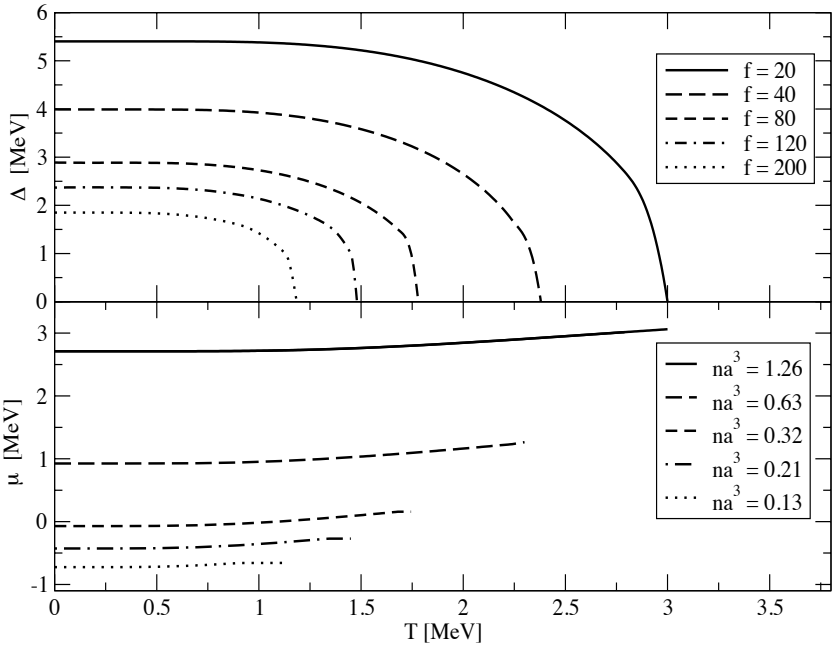

Figure 1. Dependence of the pairing gap (upper panel) and chemical potential (lower panel) on temperature for fixed values of $f = \rho_0/\rho$, where $n \equiv \rho$ denotes the baryon density and $\rho_0 = 0.16$ fm^{-3} the saturation density of symmetrical nuclear matter. Values of the dimensionless density parameter $n|a|^3$ assume a scattering length $a = 5.4$ fm.

of a dispersive fermionic background medium and attendant Pauli blocking effects. Evolution of clustering into deuteron dimers and triton and helion trimers was followed under increasing temperature and/or decreasing density. For small temperatures the quantum degeneracy is large and Pauli blocking strongly suppresses the binding energy of these clusters, which are quenched at a common critical temperature T_{cc}.

The results on pairing and bound states are combined to produce the schematic phase diagram in Fig. 2, showing several distinct regions in the $T - \rho$ plane:

G. The gaseous region above the solid critical line $T_{cc}(\rho)$ is populated by trimers, along with np dimers at lower temperatures.

B. The low-temperature, low-density domain (lower left: $\rho|a|^3 \ll 1$) contains a Bose condensate of tightly-bound deuterons.

C. The low-temperature, high-density domain (lower right: $\rho|a|^3 \gg 1$) features a BCS condensate of weakly-bound Cooper pairs.

L. The domain between the two critical lines $T_{cc}(\rho)$ and $T_{sc}(\rho)$ contains normal nucleonic $\{p, n\}$ liquid.

The superfluid phases labeled B and C are characterized by broken symmetry associated with the $\langle\psi\psi\rangle$ condensate. The transition C to B does not involve symmetry changes − it is a smooth crossover from the BCS to the BEC condensate. B → L and C → L are second-order phase transitions related to the vanishing of the condensate along the line $T_{sc}(\rho)$. The transition G → L (e.g., at vertical line) is characterized by an order parameter given by the fraction of trimers, which goes to zero at $T_{cc}(\rho)$ (tentatively second order).

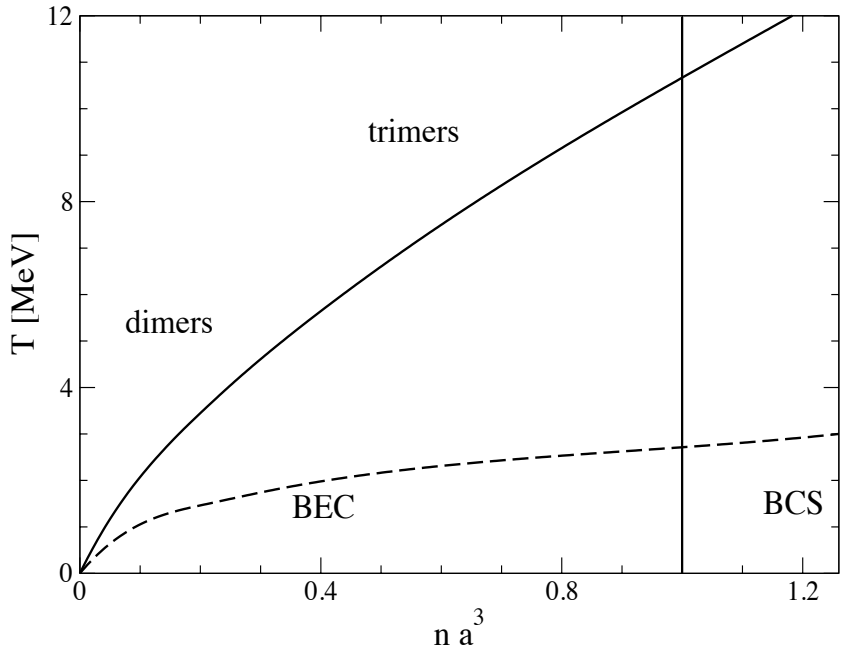

Figure 2. Phase diagram of dilute isospin-symmetric nuclear matter. Solid line: Critical temperature for extinction of three-body bound states; trimers and dimers exist above this line. Dashed line: Critical temperature for destruction of condensate. Weakly coupled BCS superfluid exists below and far to right of vertical line, Bose-Einstein condensate (BEC) of tightly bound np pairs exists below and far to the left. Dimensionless density $n|a|^3$ (with $n \equiv \rho$) as defined in Fig. 1.

3. Effects of Isospin Asymmetry on the Phase Diagram

The phase diagram of dilute nuclear matter becomes much more complex upon introduction of isospin asymmetry as another control variable, measured by

$$\alpha = (\rho_n - \rho_p)/(\rho_n + \rho_p) \tag{1}$$

in terms of neutron and proton number densities ρ_n and ρ_p. Unconventional superfluid and heterogeneous phases then emerge, largely dictated by mismatch of neutron and proton Fermi momenta k_{Fn} and k_{Fp}, which entails incomplete overlap of spherical neutron and proton Fermi spheres. As is well known, this mismatch may be mitigated by deformation of the n and p Fermi spheres so as to increase their phase-space overlap [21]. Otherwise, phase-space overlap may be enhanced by the formation of Cooper pairs having non-zero CM momentum [20, 21]. This is the alternative explored quite thoroughly in the recent work that is the primary subject of this paper. BCS pairing theory will be generalized to this case in the next section. Increase of temperature is another option for compensating the mismatch of k_{Fn} and k_{Fp}, due to the smearing of both Fermi surfaces. This effect, as well as the energetic advantage of dimerization at lower densities, gives rise to heterogeneous phases with superfluid and normal components.

The problem now has two energy scales: the pairing gap Δ in the $^3S_1$-$^3D_1$ channel, realistic NN interactions now being employed, and the shift $\pm\delta\mu = \pm(\mu_n - \mu_p)/2$ between chemical potentials of neutrons and protons. With increasing isospin asymmetry, $|\delta\mu|$ increases from zero to values of order Δ, and a sequence of unconventional phases will appear.

4. Gap Equation for Nonzero CM Momentum

A BCS suitable gap equation allowing for Cooper pairs with nonzero CM momentum may be derived in quasiparticle approximation in the framework of imaginary-time finite-temperature Green's functions and the Nambu-Gor'kov basis [2, 4, 3]. The resulting quasiparticle spectra are written in a general reference frame moving with CM momentum $\mathbf{Q}$ relative to a laboratory rest frame.

This *ab initio* many-body theory yields solutions of the form

$$G^{\pm}_{n/p} = \frac{ik_\nu \pm \epsilon^{\mp}_{p/n}}{(ik_\nu - E^{+}_{\mp/\pm})(ik_\nu + E^{-}_{\pm/\mp})}, \tag{2}$$

$$F^{\pm}_{np} = \frac{-i\Delta}{(ik_\nu - E^{+}_{\pm})(ik_\nu + E^{-}_{\mp})}, \qquad F^{\pm}_{pn} = \frac{i\Delta}{(ik_\nu - E^{+}_{\mp})(ik_\nu + E^{-}_{\pm})}, \tag{3}$$

for the normal and anomalous Green's functions, respectively, where $k = (ik_\nu, \mathbf{k})$, with $k_\nu = (2\nu+1)\pi T$, ν being any integer. There are four quasiparticle spectral branches specified by

$$\epsilon^{\pm}_{n\uparrow/\downarrow} = E_S - \delta\mu \pm E_A, \qquad \epsilon^{\pm}_{p\uparrow/\downarrow} = E_S + \delta\mu \pm E_A, \tag{4}$$

where, with $a, r \in \{+,-\}$,

$$E^a_r = \sqrt{E_S^2 + \Delta^2} + r\delta\mu + aE_A, \qquad E_S = (Q^2/4 + k^2)/2m^* - \bar{\mu}, \qquad E_A = \mathbf{k}\cdot\mathbf{Q}/2m^*. \tag{5}$$

The isospin asymmetry enters through the parameter $\delta\mu = (\mu_n - \mu_p)/2$, while $\bar{\mu}$ is the mean chemical potential.

In mean-field approximation, the anomalous self-energy (pairing gap) is expressed as

$$\Delta(\mathbf{Q}) = \frac{1}{4\beta}\int \frac{d^3k'}{(2\pi)^3}\sum_\nu V(\mathbf{k},\mathbf{k}')\mathrm{Im}[F^{+}_{np}(k'_\nu,\mathbf{k}',\mathbf{Q}) + F^{-}_{np}(k'_\nu,\mathbf{k}',\mathbf{Q}) - F^{+}_{pn}(k'_\nu,\mathbf{k}',\mathbf{Q}) - F^{-}_{pn}(k'_\nu,\mathbf{k}',\mathbf{Q})] \tag{6}$$

in terms of the above anomalous propagators, where $V(\mathbf{k},\mathbf{k}')$ is the np pairing interaction. The next steps toward deriving the gap equation as used in the numerical study of pairing in dilute nuclear matter involve (i) evaluation of the Matsubara sum over ν in the above expression, (ii) performing a partial wave expansion, and (iii) restricting attention to the ${}^3S_1$-${}^3D_1$ channel, in which the appropriate np interaction is denoted by $V_{l,l'}(k,k')$ with $l, l' = 0, 2$. Thus one arrives at

$$\Delta_l(Q) = \frac{1}{4}\sum_{a,r,l'}\int \frac{d^3k'}{(2\pi)^3}\frac{V_{l,l'}(k,k')\Delta_{l'}(k',Q)}{2\sqrt{E_S^2(k') + \Delta^2(k',Q)}}[1 - 2f(E^r_a)], \tag{7}$$

wherein $f(E^r_a) = 1/[\exp(E^r_a/T) + 1]$ and $\Delta^2 = (3/8\pi)\sum_l \Delta_l^2$.

Correspondingly, the partial number densities $\rho_{n/p}(\mathbf{Q})$ of neutrons and protons are determined in terms of normal propagators by

$$\rho_{n/p}(\mathbf{Q}) = \frac{2}{\beta}\int \frac{d^3k}{(2\pi)^3}\sum_\nu G^{+}_{n/p}(k_\nu,\mathbf{k},\mathbf{Q}) = 2\int \frac{d^3k}{(2\pi)^3}\frac{1}{2}\left[(1+\xi)f(E^{+}_{\mp}) + (1-\xi)f(-E^{-}_{\pm})\right], \tag{8}$$

where $\xi = E_S/\sqrt{E_S^2 + \Delta^2}$.

5. Calculational Specifics and Interactions Assumed

The coupled gap equations and the two density equations were solved self-consistently for a bare pairing interaction in the $^3S_1$-$^3D_1$ partial wave, as provided by a phase-equivalent in-vacuum NN interaction, namely by the Paris potential, thus implying Cooper pairing in the $S = 1$, $T = 0$ spin-isospin channel. As needed, the nuclear mean field is modeled by a Skyrme density functional, with SkIII and SLy4 parametrizations yielding nearly identical results.

Two simplifications are made:

(i) Polarization effects, i.e., medium modification of the input NN interaction (due for example to virtual exchange of density and spin-density excitations) are neglected, although they are known to be important in some regions of the phase diagram.

(ii) Apart from deuteron dimerization in the BEC phases, effects of nuclear clustering are not considered, although at somewhat higher temperatures one expects substantial populations of tritons, ^{3}He nuclei, and α particles, along with deuterons.

It should also be noted that $^1S_0$ Cooper pairing in the $S = 0$, $T = 1$ spin-isospin channel may mix and eventually replace $^3S_1$-$^3D_1$ pairing at asymptotically low T (below 0.5 MeV) and high asymmetry.

6. Free-Energy Minimization

The phase at each point in the $T - \rho$ phase diagram is determined by minimization of the free energy. In the case of pre-BEC homogeneous phases (perhaps translationally noninvariant), there are three possibilities: (i) $Q = 0$, $\Delta \neq 0$ (BCS phase), (ii) $Q \neq 0$, $\Delta \neq 0$ (LOFF phase), and (iii) $Q = 0$, $\Delta = 0$ (unpaired, normal phase). The ground state is determined by minimization of the free energy $F = E - TS$ of the superfluid ($\mathcal{S}$) or unpaired normal phase ($\mathcal{N}$) with respect to the parameter Q, where E is the internal energy determined from the Hamiltonian and S the entropy. Stability of the superfluid phase requires $F_{\mathcal{S}} < F_{\mathcal{N}}$.

As already indicated, there can also be a (pre-BEC) heterogeneous, phase-separated phase, denoted PS-BCS. Its free energy takes the form of a linear combination of superfluid and unpaired free energies,

$$\mathcal{F}(x, \alpha) = (1 - x)F_S(\alpha = 0) + xF_N(\alpha \neq 0),$$

which is to be minimized with respect to the filling fraction x of the unpaired component. The net densities of n/p per unit volume are given by $\rho_{n/p} = (1 - x)\rho^{(S)}_{n/p} + x\rho^{(N)}_{n/p}$. In the pure $\mathcal{S}$ phase, $\rho^{(S)}_n = \rho^{(S)}_p = \rho^{(S)}/2$.

7. Overview of the Phase Diagram

In this section we present an overview of the diverse phases that arise as the calculation proceeds from higher to lower densities in dilute nuclear matter at chosen isospin asymmetries $\alpha \geq 0$.

7.1. Conventional Phases

As specified, the microscopic calculation yields a smooth crossover from the pure BCS phase to an asymptotic state corresponding to a mixture of a deuteron BEC and a normal gas of the left-over unpaired neutrons. The transition from BCS to BEC is identified by two criteria: (i) The average chemical potential $\bar{\mu}$ changes its sign from positive to negative values, and (ii) The coherence length ξ of a Cooper pair becomes comparable to the interparticle distance d,

$$\xi \sim d = (3/4\pi\rho)^{1/3},$$

as ξ ranges from $\xi \gg d$ to $\xi \ll d$.

7.2. Unconventional Phases: LOFF and PS-BCS

At $\alpha \neq 0$ the LOFF state can emerge due to the energetic advantage gained with a condensate that breaks translational symmetry: Cooper pairs that carry a nonzero CM momentum $\mathbf{Q}$ can compensate for the mismatch of neutron and proton chemical potentials. The calculations reveal the existence of a LOFF-state gap of isospin-asymmetric nuclear matter in a narrow regime at relatively low T and relatively high ρ values, having a maximum at finite Q, implying maximum condensation energy for such pairs. At large α, the maximum gap occurs at large values of Q. On the other hand, at a given asymmetry, an increase of temperature shifts the gap maximum and free-energy minimum toward smaller Q. With reduction of asymmetry, increase of temperature, and/or decrease of density, the BCS phase regains favor over the LOFF phase, with PS-BCS phase having the advantage in the contest at lower temperatures.

This behavior relative to the LOFF phase is well understood in terms of the phase-space overlap of the Fermi surfaces of neutrons and protons, which increases with increasing temperature on the one hand, and with momentum Q on the other. Similarly, the PS-BCS phase, in which a standard ($^3S_1$-$^3D_1$) BCS component coexists with a normal Fermi liquid made up of the excess unpaired neutrons, is clearly favored energetically relative to pure BCS and LOFF phases at the lowest temperatures, where there is little benefit from eroded Fermi surfaces of from forfeit of translational invariance.

What remains is an account of how the BCS-BEC crossover is affected by the existence of the unconventional nuclear LOFF and PS phases at nonzero α, under decrease of system density.

8. Inventory of Condensed (and Uncondensed) Phases

With the density conveniently measured as $\log(\rho/\rho_0)$, results from the numerical calculations for different asymmetries α are plotted in the composite phase diagram of Fig. 3, which shows several distinct phases or domains:

I. We have renounced consideration of the formation of bound nuclear clusters with $A > 2$, which may occur at very low density and/or at high (but not excessively high) temperature. The homogeneous unpaired (UP) phase is then always the ground state at high temperatures $T > T_{c0}$ in the restricted domain under study, where T_{c0} is the critical temperature of the pairing transition at $\alpha = 0$ (conventional).

II. The homogeneous isospin-asymmetric BCS phase is the ground state (denoted BCS) for all densities at intermediate temperatures (conventional).

III. The LOFF phase is the ground state in a narrow $T - \rho$ strip at low temperatures and high densities (unconventional).

IV. The domain of phase separation (PS), in either PS-BCS or PS-BEC realizations, appears at low temperatures (unconventional). In the joint PS-BCS phase, one of the components is the isospin-symmetric BCS phase, while the other is the normal isospin-asymmetric phase.

V. With decreasing density and intermediate or low temperatures, the phase diagram shows two types of BCS to BEC crossovers from the asymmetrical BCS phase to the BEC phase of deuterons and an embedded normal gas of excess neutrons: (i) A transition between the homogeneous BCS/BEC phases at moderate temperatures (nominally conventional, but with a gas of leftover neutrons in the low-density limit) and (ii) a transition between the heterogeneous PS-BCS/PS-BEC phases at low temperatures (unconventional). By convention, boundaries between BCS (or PS-BCS) and BEC (or PS-BEC) phases are decided by the change of sign of the mean chemical potential $\bar{\mu}$. In the phase diagram these appear as nearly vertical lines, insensitive to α, seen in the low-ρ-low-T corner of the phase diagram.

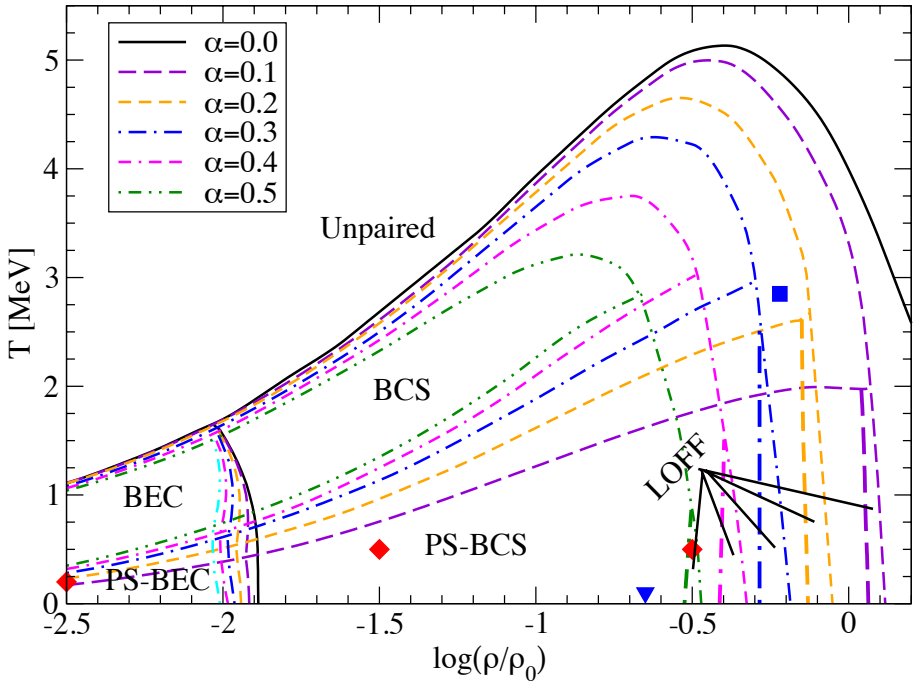

Figure 3. Phase diagram of dilute nuclear matter in the temperature-density plane at several isospin asymmetries α as indicated for the plotted lines. Four phases are represented: the normal, unpaired phase, the BCS (BEC) phase, the LOFF phase, and a PS-BCS (PS-BEC) phase. At each asymmetry there are two tri-critical points, one always being Lifshitz point. For special values of asymmetry these two tricritical points degenerate into single tetra-critical point, exemplified for $\alpha_4 = 0.255$ (marked by blue square). The LOFF phase disappears at the point $\log(\rho/\rho_0) = 0.65$ and $T = 0$ for $\alpha = 0.62$ (marked by blue triangle). Red triangles: representative points of strong, moderate, and weak coupling, left to right.

9. Special Features of the Phase Diagram

In terms of symmetries, four phases are identified: unpaired (UP), BCS/BEC, LOFF, and PS-BCS (PS-BEC). The results of the calculations performed are consistent with the transitions between BCS to BEC or between PS-BCS and PS-BEC being smooth crossovers without change of symmetry. The superfluid/unpaired phase transition and the transitions between superfluid phases are second order, except for those between PS-BCS and LOFF phases, which are of first order. At each nonzero isospin asymmetry $\alpha < 0.62$, the phase diagram exhibits two tricritical points where a simpler pairwise coexistence terminates and three different phases coexist, e.g., BCS, PS-BCS, and LOFF. One of these is always a Lifshitz point. For special values of asymmetry, the two tricritical points degenerate into a single tetracritical point; an example is shown as the blue square in Fig. 3, occurring at $\log(\rho/\rho_0) = -0.22$ and $T = 2.85$ for $\alpha = 0.255$.

10. Beyond the Phase Diagram

It is useful to distinguish three dynamical regimes:

- The weak-coupling regime (WCR) corresponds to the high-density limit where well-defined Cooper pairs are present.
- The strong-coupling regime (SCR) corresponds to the low-density limit where well-defined

deuterons are formed.

- In between: intermediate coupling regime (ICR).

The following properties of pairing and condensates in low-density nuclear matter have been examined in detail within the same calculational framework:

- Temperature and asymmetry dependence of the pairing gap, with comparison of BCS and LOFF phases.
- The kernel of the gap equation as the momentum space-wave function of the Cooper pair, with comparison of BCS and LOFF phases.
- Evolution of the Cooper-pair wave function from the WCR through the ICR to the SCR, i.e., evolution from BCS pairing to the BEC condensate of deuterons.
- Occupation numbers of neutrons and protons; their behaviors from the BCS phase in WCR, through ICR, and on to BEC in SCR; LOFF in WCR.
- Quasiparticle excitations: dispersion relations for quasiparticle spectra in the $^3S_1$-$^3D_1$ BCS condensate and in the LOFF phase; evolution of spectral branches from WCR through ICR to SCR.

We next turn to selected samples of results from these informative studies. In figures providing results in the WC, IC, and SC regimes, typical values have been selected at (T, ρ) pairs specified as follows. WCR: $T = 0.5$ MeV, $\log(\rho/\rho_0) = -0.5$. ICR: $T = 0.5$ MeV, $\log(\rho/\rho_0) = -1.5$. SCR: $T = 0.2$ MeV, $\log(\rho/\rho_0) = -2.5$.

10.1. Behavior of the Pairing Gap

Results have been obtained for the pairing gap at density $\rho = 0.1$ fm^{-1} (a) as a function of temperature for different asymmetry values, and (b) as a function of asymmetry for different temperatures (see Figs. 4 and 5). When the possibility of a LOFF phase is taken into account, these results, when plotted for each value of α, reveal different regimes at relatively low and relatively high temperature. The high-temperature segment corresponds to the BCS state, with standard temperature dependence of the gap. By contrast, in the low-temperature region below the branch point, there are two competing phases: BCS and LOFF, with very different temperature dependences of the gap function.

The quenching of the BCS gap upon decrease of T is caused by the loss of coherence among the quasiparticles as the thermal smearing of the Fermi surfaces is terminated, with the (unorthodox) consequence that for large enough asymmetries there exists a lower critical temperature $T_{c\downarrow}$.

In the plots of Fig. 5 showing Δ versus α for several chosen temperatures and fixed density, there are two curves for each T value: one in the low-α regime where only the BCS phase exists, and the other in the large-α regime where both BCS and LOFF are possible. The LOFF solution wins the competition in the latter region, since it provides larger gap values.

10.2. Kernel of the Gap Equation and Cooper-Pair Wave Function

The kernel of the gap equation,

$$K(k) = \frac{1}{2} \sum_{a,r} \frac{1}{2\sqrt{E_S^2(k) + \Delta^2(k,Q)}} [1 - 2f(E_a^r)], \tag{9}$$

is the product of the imaginary part of the retarded anomalous propagator and the Pauli operator $P_r^a = 1 - 2f(E_a^r)$. Physically, $K(k)$ can be interpreted as the momentum-space wave function of the Cooper pairs, since it obeys a Schrödinger-type eigenvalue equation in the limit of extremely strong coupling. The Pauli operator is a smooth function of momentum with a maximum at the

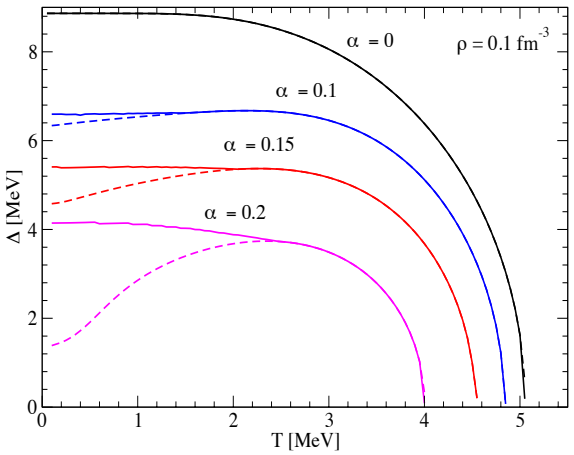

Figure 4. Gap as a function of temperature at constant density for asymmetry values $\alpha = 0.0$ (black), $\alpha = 0.1$ (blue), $\alpha = 0.15$ (red), $\alpha = 0.2$ (magenta). Results allowing for the LOFF phase are traced by solid lines, those restricted to the BCS phase, by dashed lines.

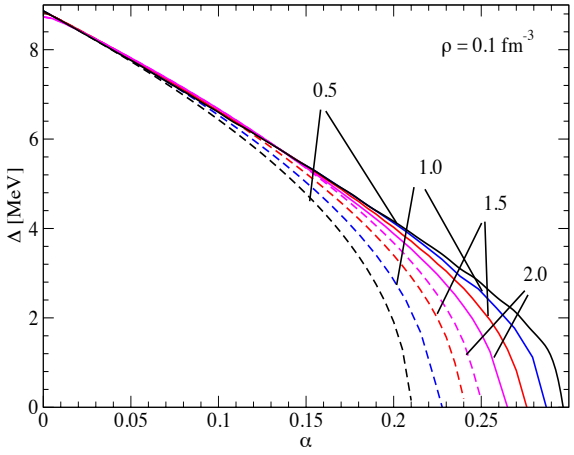

Figure 5. Gap as a function of asymmetry at constant density for temperature values $T = 0.5$ (black), $T = 1.0$ MeV (blue), $T = 1.5$ MeV (red), $T = 2.0$ MeV (magenta). Results allowing for the LOFF phase are traced by solid lines, those restricted to the BCS phase, by dashed lines.

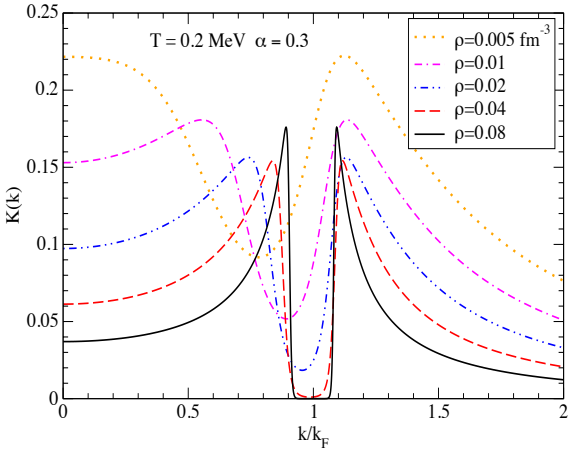

Figure 6. Dependence of the kernel $K(k)$ on momentum in units of Fermi momentum for fixed $T = 0.2$ MeV, $\alpha = 0.3$, and various densities indicated in the plot.

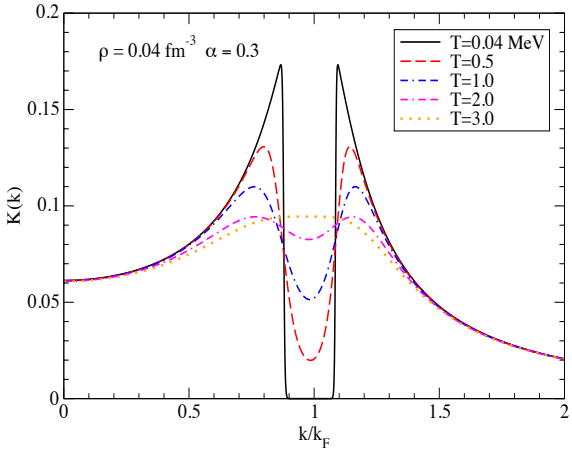

Figure 7. Dependence of the kernel $K(k)$ on momentum in units of Fermi momentum for fixed $\rho = 0.04$ fm^{-3}, $\alpha = 0.3$, and various temperatures indicated in the plot.

Fermi surface, where E_S vanishes. In practice, contributions from the two relevant excitation branches with $r \neq a$ are kept; those from the cases $r = a$ are negligible. Plots showing the momentum dependence of the kernel for asymmetry $\alpha = 0.3$ and relevant values of density and temperature are provided in Figs. 6 and 7.

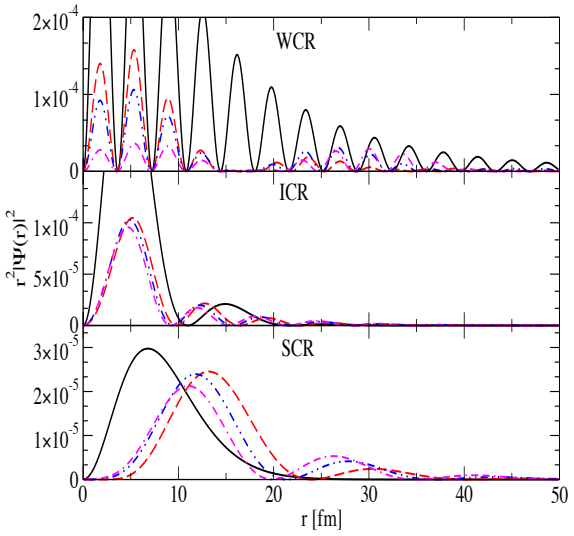

Figure 8. Dependence of $r^2|\Psi(r)|^2$ on r for the three coupling regimes. Color-coded α values: 0.0 (black), 0.1 (red), 0.2 (blue), 0.3 (magenta).

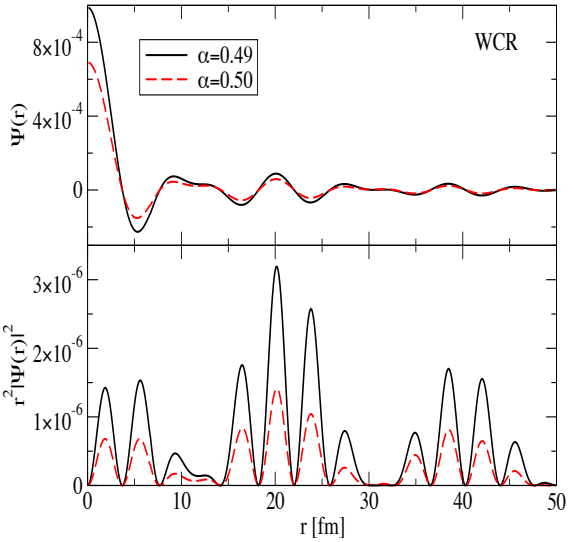

Figure 9. Dependence of $\Psi(r)$ and $r^2|\Psi(r)|^2$ on r in the WCR for two asymmetries at which the LOFF phase is the ground state.

10.3. Cooper-Pair Wave Function and Correlation Length

The superfluid coherence length ξ is directly related to the root-mean-square radius of the **r**-space Cooper-pair wave function, given by

$$\Psi(\mathbf{r}) = \mathcal{N} \int \frac{d^3p}{(2\pi)^3}[K(\mathbf{p},\Delta) - K(\mathbf{p},0)]e^{i\mathbf{p}\cdot\mathbf{r}}, \tag{10}$$

where the factor $\mathcal{N}$ ensures unit norm for $\Psi(\mathbf{r})$. The mean-square radius of the Cooper pair is then defined as

$$\langle r^2 \rangle = \int d^3r r^2 |\Psi(\mathbf{r})|^2, \tag{11}$$

and its spatial extent, the coherence length, as $\xi_{\rm rms} = \sqrt{\langle r^2 \rangle}$. In traversing the BCS-BEC crossover, the change in the coherence length tracks the change of the condensate wave function. The regimes of weak and strong coupling can be identified by comparing the coherence length, given in the BCS case by the familiar result $\xi_a = \hbar^2 k_F/\pi m^* \Delta$, to the mean distance $d = (3/4\pi\rho)^{1/3}$. Detailed computation and analysis based on these relations firmly establishes that in the BCS limit (WCR) one is dealing with a coherent state whose wave function oscillates over many periods characterized by k_F^{-1}. In the opposite limit (SCR), the wave function is concentrated around the origin, indicating that one is dealing with a Bose condensate of strongly bound states: deuterons. Plots illustrating the behavior of $r^2|\Psi(\mathbf{r})|^\mathbf{2}$ versus r in the different coupling regimes and for selected asymmetries α are provided in Figs. 8 and 9.

10.4. Occupancies, Excitations, and Pauli Blocking Effects

Analysis of the kernel $K(k)$, the p and n occupation probabilities, and quasiparticle dispersion relations reveal prominent effects of Pauli blocking (the "breach"). Summarizing the phenomena occurring in the different coupling regimes, we find

- WCR: At large asymmetries, the minority component is expelled from the blocking region ($n_p \approx 0$), while the majority component is maximally occupied ($n_n/2 \approx 1$). The "breach" is filled in with increasing T.

- WCR: The LOFF phase appearing in this regime largely mitigates the blocking mechanism by allowing for a non-zero CM momentum of the condensate. Accordingly, all intrinsic properties are much closer to those of the isospin-symmetric BCS phase.
- WCR: In the small-α limit, the occupation numbers are clearly fermionic, with some diffuseness due to the temperature.
- ICR: The fermionic nature of the occupation numbers is lost, a Fermi surface cannot be identified, and no "breach" appears.
- ICR: For large α values, the occupation numbers become non-monotonic; for the minority component this is a precursor of a change in the topology of the Fermi surface in the transition ICR $\rightarrow$ SCR.
- SCR: the occupation numbers and other properties are consistent with a BEC of strongly-coupled pairs (deuterons). At large asymmetries, the Fermi sphere of the minority component in the WCR has evolved into a shallow shell structure.
- SCR: long-range coherence of the condensate is lost.
- WCR $\rightarrow$ ICR $\rightarrow$ SCR: The quasiparticle dispersion relation changes in form from that corresponding to the existence of a Fermi surface to one that is minimal at $k = 0$, independent of isospin asymmetry.
- With increasing α, the proton component acquires points with zero excitation energy, as in gapless superconductivity. The occupation numbers reach a maximum at finite k and reflect a change of topology: from the filled Fermi sphere to one with an empty "core."

11. The Missing Ingredient: Formation of Nuclear Clusters

The matter in supernova envelopes is (i) at finite isospin asymmetry (though remaining quite small compared to its values in the crust of a neutron star), and (ii) at relatively high temperatures compared to those considered in the present study. This environment could support the existence of a substantial population of nuclear clusters besides deuterons, notably tritons, ^{3}He nuclei, and alpha particles. The α particles may form a BEC at sufficiently low temperatures. The extent to which the presence of such clusters will modify the structure of the phase diagram constructed so far remains to be determined at a comparable level of microscopic precision. Additionally, formation of neutron dimers in the nuclear medium remains a tantalizing possibility, which will be explored schematically in the second part of this review.

12. Framework for BCS Pairing Versus Hidden Dimer State: "Take One"

The NN interaction in the $^1S_0$ partial wave, having a scattering length $a = -18.95$ fm and a strong resonance at the tiny energy of 0.067 MeV, just barely fails to support a bound state. Although this hypothetical dineutron cannot exist in vacuum, there remains a tantalizing potential for it to be bound in a nuclear medium and even in pure neutron matter. For example, it would take an effective, in-medium mass M^* of about 5% over the bare mass M for a dineutron to bind in the pure neutron system. One could think of such a dineutron as a nuclear analog of the polaron of solid-state physics, which also has no existence in vacuum.

Recently, Eckhard Krotscheck's quantum many-body group at Buffalo [18] has developed and executed a powerful *ab initio* approach within correlated-basis theory that is capable of quantitative prediction of the ground-state properties of strongly interacting Fermi systems in the low-density regime, with errors in the ground-state energy below 2%. For two-body interactions qualitatively similar to the S-wave neutron-neutron potential, these authors have exploited rigorous variational aspects of this approach to demonstrate the existence of a robust singularity at low (but not asymptotically low) density that is plausibly associated dimerization of the system driven by phonon exchange. This behavior is analogous to what occurs at

zero density when the in-vacuum scattering length diverges; accordingly, it is interpreted in terms of divergence of a well-defined in-medium scattering length at finite density. On a more phenomenological plane, it is important to highlight not only historical [23] early interest in possible existence of a dineutron, but more significantly an extensive body of recent theoretical and experimental work [24], respectively predicting and providing evidence for strong dineutron correlations in finite nuclei or nuclear matter, even suggesting a tendency toward Bose-Einstein condensation of long-lived dineutrons.

Our objective for this section of the review and the next is to furnish a schematic framework [5, 25] for the emergence of a hidden dimer state in homogeneous Fermi matter (potentially a dineutron in the case of realistic nuclear matter), which competes energetically with BCS pairing states, both conventional and unconventional. The present analysis follows the same paths as explored in [5], but uncovers additional subtleties beyond what is revealed in that work. In some important aspects, this treatment supplements the *ab initio* study carried out in [18] within the method of correlated basis functions. The analysis is primarily based on the Thouless criterion for determination of the critical temperature for the onset or termination of pairing correlations. The Thouless criterion [26, 16] centers on the behavior of the linear integral equation

$$\mathcal{T}(p,T) = -\int V(p,p_1)\frac{\tanh\left(\epsilon(p_1)/2T\right)}{2\epsilon(p_1)}\mathcal{T}(p_1,T)d\upsilon_1. \tag{12}$$

for the finite-temperature T-matrix (denoted here by $\mathcal{T}$), stating that if it does not have a pole at temperature T, this temperature lies above above the transition temperature. The single-particle spectrum appearing in this equation is given by $\epsilon(p) = p^2/2M - \mu$, with M the bare mass and μ the chemical potential.

Analysis of Eq. (12) is expedited by decomposing the momentum-space pairing interaction $V(p_1,p_2)$ identically into a separable component and a remainder $R(p_1,p_2)$ that vanishes when either momentum argument is on the Fermi surface:

$$V(p_1,p_2) = V_F\phi(p_1)\phi(p_2) + R(p_1,p_2). \tag{13}$$

The latter property is guaranteed by the choice $\phi(p) = V(p,p_F)/V_F$, with $V_F = V(p_F,p_F)$. Inserting this expression into Eq. (12), simple algebra leads to an equivalent set of two coupled equations. The first is a linear integral equation for the shape $\chi(p) = \mathcal{T}(p)/\mathcal{T}(p_F)$ of $\mathcal{T}$ in momentum space:

$$\chi(p) = \phi(p) - \int R(p,p_1)\frac{\tanh\left(\epsilon(p_1)/2T\right)}{2\epsilon(p_1)}\chi(p_1)d\upsilon_1, \tag{14}$$

while the second equation takes the form

$$-\frac{1}{V_F} = \int \phi(p)\frac{\tanh\left(\epsilon(p)/2T\right)}{2\epsilon(p)}\chi(p)d\upsilon. \tag{15}$$

Due to the imposed behavior of the remainder function $\mathcal{R}$, the description of singular behavior in the Cooper pairing channel is isolated in the second equation. The same tactic was invoked to develop an efficient and accurate procedure [27] for solving BCS-type gap equations in those cases where the pairing interaction contains a strong inner repulsion in coordinate space. Widely used versions of the NN interaction, such as the Reid soft-core and Argonne V18, are of this character.

Introducing the difference $\eta(p) = \chi(p) - \phi(p)$, the second equation may be rewritten as

$$-\frac{1}{V_F} = I_{11}(T) + \int \phi(p)\frac{\tanh\left(\epsilon(p)/2T\right)}{2\epsilon(p)}\eta(p)d\upsilon, \tag{16}$$

where

$$I_{11}(T) = \int \phi(p) \frac{\tanh\left(\epsilon(p)/2T\right)}{2\epsilon(p)} \phi(p) d\upsilon, \tag{17}$$

while $\eta(p)$ obeys an integral equation replacing (14), viz.

$$\eta(p,T) = -\int R(p,p_1) \frac{\tanh\left(\epsilon(p_1)/2T\right)}{2\epsilon(p_1)} \left(\phi(p_1) + \eta(p_1,T)\right) d\upsilon_1. \tag{18}$$

At the bifurcation point $T = 0$, the first term on the right side of Eq. (16), i.e., $I_{11}(T)$, diverges logarithmically, behaving essentially as $0.5N(0)\ln(\epsilon_c/T)$. Therefore a solution $T = 0$ exists only if the second term *also* diverges at this point.

To confirm that a compensating divergence occurs, we expand the function $\eta(p)$ in a basis formed by the eigenfunctions $\zeta_n(p)$ of the kernel $R(p,p';\rho)L(p,0)$ involving the propagator

$$L(p,\omega) = -(1-2n(p))/(\omega - 2\epsilon(p) - i\delta\,\mathrm{sgn}(p-p_F)). \tag{19}$$

The expansion is dominated by the contribution from the eigenfunction $\zeta_0(p)$ belonging to the lowest eigenvalue σ_0 of this kernel, which satisfies

$$\zeta_0(p) = -\sigma_0 \int R(p,p_1,\rho) \frac{1}{2|\epsilon(p_1)|} \zeta_0(p_1) d\upsilon_1. \tag{20}$$

Thus we write

$$\eta(p,T) = \eta_0(T)\zeta_0(p) + \vartheta(p), \tag{21}$$

where the remainder $\vartheta(p)$ vanishes on the Fermi surface. Inserting this expression into the integral equation (18) for $\eta(p,T)$ and collecting all terms having $\eta_0(p,T)$ as a factor on the left, we have

$$\eta_0(T) \left(\zeta_0(p) + \int R(p,p_1) \frac{\tan(\epsilon(p_1)/2T)}{2\epsilon(p_1)} \zeta_0(p_1)\, d\upsilon_1\right) = Z(p), \tag{22}$$

where

$$Z(p) = -\vartheta(p) - \int R(p,p_1) \frac{\tan(\epsilon(p_1)/2T)}{2\epsilon(p_1)} (\phi(p_1) + \vartheta(p_1))\, d\upsilon_1. \tag{23}$$

It is convenient to use the eigenvalue equation (20) for ζ_0 to rewrite the left side of Eq. (22) as

$$\eta_0(T) \left(\frac{\kappa}{\sigma_0}\zeta_0(p) + \int R(p,p_1)\mathcal{D}(p_1,T)\zeta_0(p_1) d\upsilon_1\right) = Z(p), \tag{24}$$

where

$$\mathcal{D}(p,T) = \frac{\tanh\left(\epsilon(p)/2T\right)}{2\epsilon(p)} - \frac{1}{2|\epsilon(p)|} \tag{25}$$

and $\kappa \equiv \sigma_0 - 1$. Next, both sides of this result are multiplied by the product $\zeta_0(p)/(2|\epsilon(p)|)$, and the momentum integration is performed. The operator R may be eliminated from (22) with the aid of (20) to obtain

$$\eta_0(T) = (\kappa + \gamma(T))^{-1} I_{10}/I_{00}, \tag{26}$$

where $I_{00} > 0$ is given by

$$I_{00} = \int \zeta_0(p) L(p,0) \zeta_0(p)\, d\upsilon, \tag{27}$$

while

$$\gamma(T) = I_{00}^{-1} \int \zeta_0(p) \left(\frac{\tanh(\epsilon(p)/2T)}{2\epsilon(p)} - \frac{1}{2|\epsilon(p)|}\right) \zeta_0(p)\, d\upsilon \tag{28}$$

and

$$I_{10} = \sigma_0 \int \zeta_0(p) \frac{1}{2|\epsilon(p)|} Z(p)\, d\upsilon. \tag{29}$$

Equation (26) is the main result of this analysis.

To demonstrate that the sign of $\gamma(T)$ is positive, as required, the integrand in Eq. (28) is rearranged to write

$$\gamma(T) \propto \int \zeta_0^2(p) \frac{\tanh(|\epsilon(p)|/2T) - 1}{2|\epsilon(p)|} d\upsilon. \tag{30}$$

Since $\zeta_0(p)$ vanishes at the Fermi surface like $\epsilon(p)$, we may conclude that $\gamma(T) = \gamma T^2$, where henceforth γ is a positive constant.

Considering next the integral I_{10}, the explicit form for $Z(p)$ is inserted into its integrand. Noting that that the terms involving the remainder ϑ essentially cancel one another, we may then take

$$I_{10} = \int \zeta_0(p) \frac{1}{2|\epsilon(p)|} \phi(p) d\upsilon. \tag{31}$$

Since $\gamma(T)$ vanishes as T^2 for $T \to 0$, we see from Eq. (26) that the coefficient $\eta_0(T)$ does in fact diverge together with the function $\eta(p)$ itself at the critical point where $\kappa = \sigma_0 - 1$ changes sign.

We are now ready to substitute the result (26) into the dispersion relation (16). Implementing an energetic cutoff $\epsilon_c \sim \epsilon_F^0$ in the result, we then arrive at

$$\frac{1}{2} \ln(\epsilon_c/T) = \frac{1}{\lambda} - \frac{\nu^2}{\kappa(\rho) + \gamma T^2}, \tag{32}$$

where it is to be understood that all minor corrections are included in the effective pairing constant denoted λ.

This analysis was performed with the case ($\lambda > 0$, $\kappa < 0$) in mind. Near the critical density ρ_t, the "stiffness" parameter κ, being small and negative, behaves as

$$\kappa \sim -|(\partial\kappa/\partial\rho)_t|(\rho_t - \rho). \tag{33}$$

For small $|\rho_t - \rho|$, the contribution of the $1/\lambda$ term on the right side of Eq. (32) can be neglected, and we find

$$T_1 \propto \exp[-(a\rho_t)/(\rho_t - \rho)], \tag{34}$$

where a is a numerical constant. Since the BCS constant λ does not enter this result, we infer that the solution so obtained does not belong to the BCS type.

However, there is in fact a second root of Eq. (32), lying at temperatures $T_2 > \sqrt{|\kappa|/\gamma} > T_1$. To assess its location, we set $\kappa = 0$ in Eq. (32) to write

$$\frac{\lambda\gamma}{2} T^2 \ln(\epsilon_c/T) = \gamma T^2 - \lambda\nu^2. \tag{35}$$

The solution of this equation has the form

$$T_2{}^2 = \lambda\nu^2/\gamma + O(\lambda^2 \ln\lambda). \tag{36}$$

Since the result (36) depends explicitly on the BCS constant λ, it is this solution that corresponds to Cooper pairing. We conclude that the dineutron state loses in its competition with the BCS-like state (36), as long as the magnitude of the critical parameter $|\kappa|$ remains small.

The situation at $T \to 0$ changes completely when $|\kappa|$ increases beyond $\lambda\nu^2$, for then the first term on the right side of Eq. (32) prevails over the second. As a result, the first root of

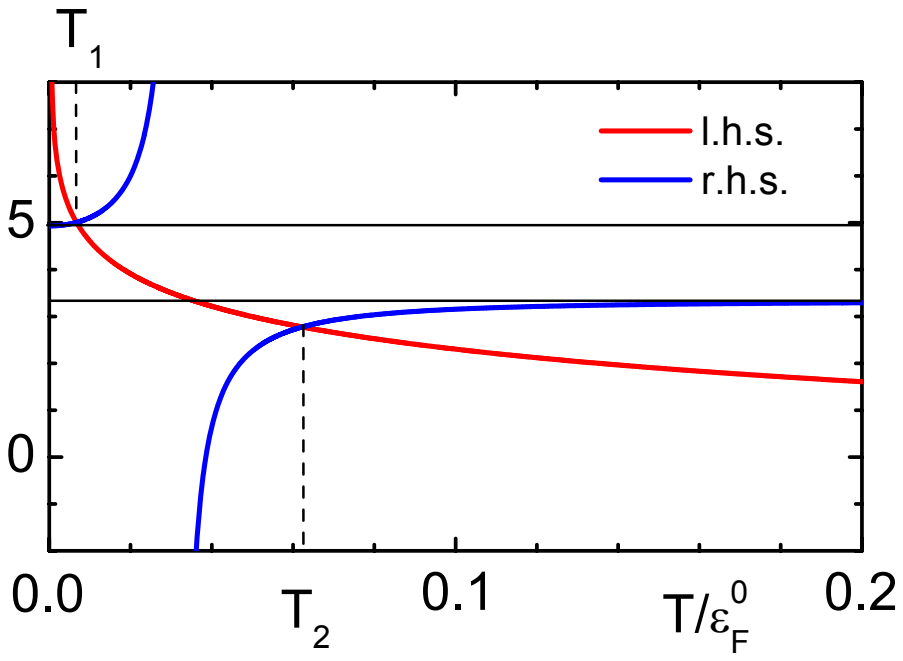

Figure 10. Graphical demonstration of two solutions of Eq. (32). Model parameters adopted: $\lambda = 0.3$, $\nu = 0.04$, $\kappa = -0.001$, $\gamma = (\epsilon_F^0)^{-1/2}$, $\epsilon_c = \epsilon_F^0$. The in-medium dineutron solution rather than the BCS solution ensures the maximum critical temperature for termination of pairing correlations provided $|\kappa| > \lambda\nu^2$; otherwise the BCS solution still holds.

this equation has the standard BCS form $T_1 = \epsilon_c \exp[-1/\lambda]$. However, as before there exists a different and larger root, determined by the relation

$$T_2 = T_{nn} = \sqrt{(|\kappa| + \lambda\nu^2)/\gamma} \simeq \sqrt{|\kappa|/\gamma}, \tag{37}$$

implying that the corresponding solution is of dineutron character. Thus, at sufficiently large $|\kappa|$ the dineutron state wins the contest for survival.

Fig. 10 shows a graphical solution of the key relation (32) derived above, the running variable T being measured in units of $\epsilon_F^0 = p_F^2/2M$. The left side of this equation, plotted versus T, is traced by the red line, while the right side is drawn as two disjoint blue lines. Model inputs are stated in the figure caption. The two crossing points determine two critical temperatures, T_1 and T_2, with $T_2 > T_1$.

13. Framework for BCS Pairing Versus Hidden Dimer State: "Take Two"

We now expand the analysis from the case ($\lambda > 0$, $\kappa < 0$) to the other quadrants of the $\lambda - \kappa$ parameter plane. The strategy now is to track the location of the Cooper singlet-channel pole of the zero-temperature scattering amplitude in the normal state of the homogeneous many-fermion system. We pursue this task based on the Bethe-Salpeter equation for the corresponding vertex part $\mathcal{K}_{\alpha\beta}(\mathbf{p}, \omega) = \mathcal{K}(\mathbf{p}, \omega)(\tau_2)_{\alpha\beta}$. Here α, β are spin indices, $\mathbf{p}$ is the momentum of the incoming particle (its target having momentum $-\mathbf{p}$), and ω is the total two-particle energy measured from 2μ. The equation ready for analysis now reads

$$\mathcal{K}(p, \omega) = -\int V(p, p_1) L(p_1, \omega) \mathcal{K}(p_1, \omega)\, d\upsilon_1, \tag{38}$$

where $V(p,p_1)$ represents the block of diagrams irreducible in the particle-particle channel (here just the pairing interaction) and $L(p,\omega)$, again given by Eq. (19), is the particle-particle propagator in the normal ground state. The analysis of the integral equation (38) now proceeds essentially in parallel with that carried out for Eq. (12). We bypass the lengthy details and move immediately to the final result for the basic dispersion equation, whose analytic continuation to the complex-ω plane yields

$$\frac{1}{2}\left(\ln\frac{\epsilon_c}{\omega}+i\frac{\pi}{2}\right)=\frac{1}{\lambda}-\frac{\nu^2}{\kappa+B(\omega)}, \tag{39}$$

where $\nu^2=I_{10}^2/I_{00}N(0)$, with $N(0)$ denoting the normal density of states. The function $B(\omega)$ is given by

$$B(\omega)=-(I_{00})^{-1}\int\zeta_0(p)\delta L(p,\omega)\zeta_0(p)\,d\upsilon, \tag{40}$$

with $\delta L(p,\omega)=L(p,\omega)-L(p,0)$. Setting $\Omega=i\omega$ in Eq. (39), we arrive at the general formula for determination of the pairing-gap proxy Ω,

$$\frac{1}{2}\ln\frac{\epsilon_c}{\Omega}=\frac{1}{\lambda}-\frac{\nu^2}{\kappa+B\Omega^2\ln(\epsilon_c/\Omega)} \tag{41}$$

with $B>0$.

These results prepare us to uncover systematically the nature of pairing solutions in relevant domains of the $\lambda-\kappa$ plane, while acknowledging that in a *realistic* two-nucleon interaction these two parameters actually constrain one another. (We note that the quadrant ($\lambda<0$, $\kappa>0$) is empty of solutions since the right side of Eq. (41) is never positive.)

- *Quadrant* ($\lambda>0$, $\kappa>0$). The effect of the second term on the right side of Eq. (41), proportional to ν^2, amounts just to a renormalization of the coupling constant λ in the first term. Only the BCS solution survives in this case.
- *Quadrant* ($\lambda>0$, $\kappa<0$). This case has been dealt with earlier in the context of the Thouless criterion. The parameter κ goes negative at densities below some threshold density ρ_t, thereby triggering the onset of the dineutron state. As already established above, two different solutions exist in this quadrant, a BCS solution and another corresponding to a hidden dineutron state. It is informative to track the trajectories of both roots $\Omega_{1,2}$ as functions of λ. As λ goes to zero, the left root (nearest the origin) has the behavior $\Omega_1\propto e^{-2/\lambda}$, with $\Omega_1(0)=0$. This is obviously the ordinary BCS root. In the same limit, the other root, Ω_2, is situated close to $\sqrt{|\kappa|/B}$ and is clearly of non-BCS character. With increasing λ, both roots move away from the origin. It should be emphasized that in the analysis performed, both parameters λ and κ are assumed to remain small to assure the smallness of the roots, but with this proviso the analysis performed is self-consistent. As the roots evolve with increasing λ, the two solutions switch ascendancy in the region where $\lambda\nu^2\simeq|\kappa|$. Thus we find that the dineutron state wins the competition with the BCS state only if the BCS coupling constant is rather small.
- *Quadrant* ($\lambda<0$, $\kappa<0$). Here only the root

  $$T_{nn}^2=(|\kappa|-|\lambda|\nu^2)/\gamma \tag{42}$$

  survives, but it exists only in the limit of sufficiently large $|\kappa|>|\lambda|\nu^2$. Evidently, this solution is of dineutron character.

14. Conclusions and Outlook

In this mini-review we have discussed some recent (and not so recent) advances toward the goal of a comprehensive understanding of the phase diagram of nuclear matter in the low-density regime below about half the saturation density of heavy nuclei. In this density region one may safely regard neutrons and protons as the basic constituents, interacting through two-nucleon potentials constrained by nucleon-nucleon scattering data and binding energies of light nuclei (deuteron, triton, etc.). An *ab initio* many-body approach has been applied in a quantitative exploration of the temperature-density ($T-\rho$) phase diagram of this apparently well-defined quantum many-body system [4], focusing (a) on its dependence upon isospin asymmetry and (b) simultaneously on the roles played by pairing and the BCS-BEC crossover from Cooper pairs to bound bosonic dimers (deuterons). In addition to conventional BCS pairing, its competition with unconventional LOFF pairing (in which the Cooper pairs have finite total momentum) has been treated in some detail. Away from isospin symmetry, the heterogeneous phase which combines symmetrical superfluid and asymmetric normal matter may have lowest free energy. This possibility has been taken into consideration in the numerical calculations, with the finding that two-phase mixtures are favored over the homogeneous phases at the lowest temperatures and no-to-high density, where one of the components accommodates the excess neutrons.

The major portion of this review (Secs. 2-10) has dealt with the $T-\rho$ phase diagram of dilute nuclear matter in its dependence on isospin. In Secs. 12 and 13 the focus has been shifted to another intriguing aspect of the nuclear-matter problem. Restricting attention to pure neutron matter for simplicity, this is the possibility of unconventional pairing involving the emergence of neutron dimers, i.e., dineutrons, in some density range (obviously not including $\rho \to 0$). In turn, this eventuality raises the question of whether there is a corresponding BCS-BEC transition in pure neutron matter.

A very recent study carried out by some of us [19] has a bearing on these issues. Our initial study concentrated on the T-ρ phase diagram of neutron matter including only homogeneous and isotropic phases indexed by a spin-polarization parameter. The resulting diagram resembles that of asymmetrical nuclear matter because of the analogy between nuclear matter at non-zero isospin asymmetry and pure neutron matter at non-zero spin asymmetry. An essential distinction between the phase diagrams of these systems stems from the fact that two neutrons are not bound in vacuum, whereas a neutron and a proton bind into the deuteron in free space. Accordingly, pure neutron matter cannot, in the strict sense, undergo a BCS-BEC crossover from the $^1S_0$ BCS superfluid existing at higher densities, to a BEC condensate of neutron dimers at asymptotically low density. The end state must be a neutron gas. Nevertheless, the many-body calculations carried out recently by Stein et al. [19] give clear evidence of a BCS-BEC *precursor* and thus confirm earlier findings of various authors obtained at zero spin polarization (see [19] for references). The existence of a BCS-BEC precursor is revealed, for example, by the attainment of Cooper-pair correlation lengths comparable to the interparticle distance. This behavior must be attributed to the strongly resonant character of the nn interaction at low densities, where the $^1S_0$ component is dominant.

This discourse impels us to ponder the content of Secs. 12 and 13, which provide a schematic framework for understanding the emergence of unconventional types of pairing (notably, a "hidden dineutron state") along with the conventional BCS solution. A systematic classification of such solutions is achieved in terms of two parameters: a familiar coupling parameter λ and a so-called stiffness parameter κ. As introduced, these parameters would be responsible for subsuming the effects of such complications relative to basic, bare-interaction nuclear BCS theory as (i) medium-induced corrections to the in-vacuum pairing interaction (coming from exchange of density and spin-density fluctuations, for example) and (ii) non-trivial momentum dependence of the resulting dressed interaction. (Attention should also be given to self-energy corrections.) The first category of effects ("polarization corrections") is absent in the many-body

treatment underlying the results presented in Secs. 2-10 and in [4, 19].

The recent, seminal work of Fan et al. [18] does consistently incorporate such effects in a quantitatively precise *ab initio* many-body approach developed within correlated basis theory. This approach has been exhaustively applied in a study correlations in the low-density, strongly interacting Fermi gas that addresses its Fermi-liquid state and BCS pairing, as well as dimerization induced by phonon exchange. Application of this method to neutron matter has the potential of resolving the fate of the dineutron, which may well depend (perhaps counterintuitively) on the hardness of the inner repulsion of the $^1S_0$ neutron-neutron interaction.

Acknowledgments

MS acknowledges support from the HGS-HIRe graduate program at Frankfurt University. AS is supported by the Deutsche Forschungsgemeinschaft (Grant No. SE 1836/3-1) and by the NewCompStar COST Action MP1304. XGH is supported by Fudan University Grant EZH1512519 and Shanghai Natural Science Foundation Grant No.14ZR1403000. Additionally, this research was partially supported by RFBR grants 13-02-00085, 14-02-00107, and 15-02-06261, and by grant NS-932.2014.2 from the Russian Ministry of Sciences. VAK thanks the McDonnell Center for the Space Sciences for timely support. JWC is indebted to the University of Madeira and its Centro de Ciências Matemáticas for gracious hospitality during his sabbatical residency.

References

[1] Sedrakian A and Clark JW 2006 *Phys. Rev.* C **73** 035803
[2] Stein M, Huang X-G, Sedrakian A, and Clark J W 2012 *Phys. Rev.* C **86** 062801(R)
[3] Stein M, Sedrakian A, Huang X-G, Clark J W, and Röpke G 2014 *J. Phys. Conf. Ser.* **496** 012008
[4] Stein M, Sedrakian A, Huang X-G, and Clark J W 2014 *Phys. Rev.* C **90** 065804
[5] Khodel V A, Clark J W, Shaginyan V R, and Zverev M V 2014 *Physics of Atomic Nuclei* **77** 1145
[6] Eagles D M 1969 *Phys. Rev.* **186** 456
[7] Nozières P and Schmitt-Rink S 1985 *J. Low Temp. Physics* **59** 195 1409.5649
[8] Alm T, Friman B L, Röpke G, and Schulz H 1993 *Nucl. Phys.* A **551** 45
[9] Baldo M, Lombardo U, and Schuck P 1995 *Phys. Rev.* C **52** 975
[10] Stein H, Schnell A, Alm T and Röpke G 1995 Zeits. f. Physik A **351** 295
[11] Lombardo U and Schuck P 2001 *Phys. Rev.* C **63**, 038201
[12] Mao S, Huang X, and Zhuang P 2009 *Phys. Rev.* C **79** 034304
[13] Heckel S, Schneider P P, and Sedrakian A 2009 *Phys. Rev.* C **80** 015805
[14] Huang X-G 2010 *Phys. Rev.* C **81** 034007
[15] Jin M, Urban M, and Schuck P 2010 *Phys. Rev.* C **82** 024911
[16] Ramanan S and Urban M 2013 *Phys. Rev.* C **88** 054315
[17] Sedrakian A 2013 *J. Phys. Conf. Ser.* **413** 012024
[18] Fan H H, Krotscheck E, Lichtenegger T, Mateo D, and Zillich R E 2015 *Phys. Rev.* A **92** 023640
[19] Stein M, Huang X-G, Sedrakian S, and Clark J W 2015 Spin-polarized neutron matter, critical pairing and BCS-BEC precursor *Preprint* nucl-th/1510.06000
[20] Fulde Peter and Ferrell R A 1964 *Phys. Rev.* **135** A 55; Larkin A I and Ovchinnikov Yu N 1964 Zh. Eksp. Teor. Fiz. 47: 1136
[21] Sedrakian A and Clark J W, in *Pairing in Fermionic Systems: Basic Concepts and Modern Applications* Eds Sedrakian A, Clark J W and Alford M (World Scientific, Singapore, 2006) 135
[22] Malfliet R A and Tjon J A 1969 *Nucl. Phys.* A **127** 161
[23] Feather N 1948 *Nature* **162** 213
[24] Ieki K et al 1996 *Phys. Rev.* C **54**, 1589; Matsuo M, Mizuyama K and Serizawa Y 2005 *Phys. Rev.* **71** 064326; Hagino K and Sagawa H 2005 *Phys. Rev.* C **72** 044321; Hagino K, Sagawa H, Carbonell J and Schuck P 2007 *Phys. Rev. Lett.* **99** 022506; Kanada-En'yo Y 2007 *Phys. Rev.* C **76** 044323; Isayev A A 2008 *Phys. Rev.* C **78** 014306; Papadimitriou G et al 2011 *Phys. Rev.* C **84** 051304(R); Sun T T, Sun B Y and Meng Ji 2012 *Phys. Rev.* C **86** 014305
[25] Khodel V A 1997 *Yad. Fiz.* **60** 1137
[26] Thouless D J 1960 *Ann. Phys.* (N.Y.) 553
[27] Khodel V A, Khodel V V, and Clark, J W 1996 **Nucl. Phys.** A **598** 390